Multi-Resolution Cell Orientation Congruence Descriptors for Epithelium Segmentation in Endometrial Histology Images

Guannan Li, Shan E. Ahmed Raza, Nasir M. Rajpoot

PII: S1361-8415(17)30015-4
DOI: 10.1016/j.media.2017.01.006
Reference: MEDIMA 1221

To appear in: *Medical Image Analysis*

Received date: 2 September 2016
Revised date: 27 November 2016
Accepted date: 19 January 2017

Please cite this article as: Guannan Li, Shan E. Ahmed Raza, Nasir M. Rajpoot, Multi-Resolution Cell Orientation Congruence Descriptors for Epithelium Segmentation in Endometrial Histology Images, *Medical Image Analysis* (2017), doi: 10.1016/j.media.2017.01.006

Highlights

- A novel descriptor for segmentation of luminal and glandular epithelium.
- The descriptor exploits the relatively similar orientation of epithelial cells.
- Multi-resolution extension of the proposed descriptor to improve the results.
- Detailed experimentation on a large dataset and on choice of neighbourhood.

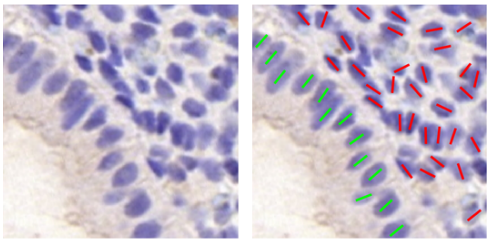

(a) (b)

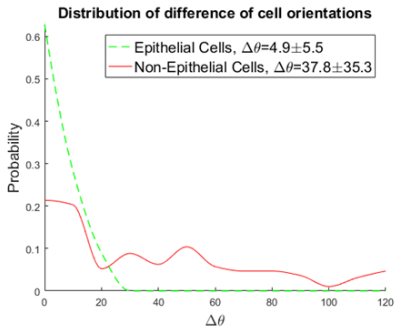

(c)

Multi-Resolution Cell Orientation Congruence Descriptors for Epithelium Segmentation in Endometrial Histology Images

Guannan Li[a], Shan E Ahmed Raza[a], Nasir M. Rajpoot[a,b]

[a]*Department of Computer Science, University of Warwick, Coventry, CV4 7AL, UK.*
[b]*Department of Pathology, University Hospitals Coventry and Warwickshire, Coventry, CV2 2DX, UK.*

Abstract

It has been recently shown that recurrent miscarriage can be caused by abnormally high ratio of number of uterine natural killer (UNK) cells to the number of stromal cells in human female uterus lining. Due to high workload, the counting of UNK and stromal cells needs to be automated using computer algorithms. However, stromal cells are very similar in appearance to epithelial cells which must be excluded in the counting process. To exclude the epithelial cells from the counting process it is necessary to identify epithelial regions. There are two types of epithelial layers that can be encountered in the endometrium: luminal epithelium and glandular epithelium. To the best of our knowledge, there is no existing method that addresses the segmentation of both types of epithelium simultaneously in endometrial histology images. In this paper, we propose a multi-resolution Cell Orientation Congruence (COCo) descriptor which exploits the fact that neighbouring epithelial cells exhibit similarity in terms of their orientations. Our experimental results show that the proposed descriptors yield accurate results in simultaneously segmenting both luminal and glandular epithelium.

Keywords: Histology image analysis, epithelium segmentation, recurrent miscarriages, digital pathology.

1. Introduction

Digital pathology offers several advantages over the age-old tissue slide analysis under the microscope by converting tissue slides into high-resolution microscopic image of the whole slide. One of these advantages is the seamless transfer and manipulation of digitised images via computer algorithms (Gurcan et al. (2009)). Indeed, histology image analysis has been tipped to hold the key to providing the much needed added value to digital pathology (Snead et al. (2015)). Computers are very efficient in performing repetitive tasks such as cell counting and can be used to improve the efficiency of routine clinical diagnosis. One such problem is counting the ratio of uterine natural killer (UNK) cells to stromal cells in endometrial biopsies.

UNK cells are immune cells in the womb lining that normally make up no more than 5% of all cells. It has recently been shown by Quenby et al. (2009) that an over-presence of UNK cells leads to recurrent miscarriage. Women with relatively high ratio of UNK to stromal cells are more likely to have a live birth if given glucocorticoids in lieu of placebo Tang et al. (2013). Thus UNK testing plays a significant role in clinical diagnosis of recurrent miscarriages. A diagnosis protocol devised by Quenby et al. (2009) calculates the ratio of UNK cells to stromal cells in histology images of endometrial tissue slides stained with Haematoxylin and CD56, which stains UNK cells brown when used with DAB staining. Consequently, the number of UNK and stromal cells must be counted. Counting stromal cells is challenging in that these cells show the same stain colour as epithelial cells, and both of them have a variety of morphological shapes and sizes, therefore it is difficult to distinguish between these two types using standard machine learning approaches Arif and Rajpoot (2007). Epithelial cells are very similar in appearance to stromal cells but they only appear in glandular and luminal epithelial regions. Therefore, we propose to segment the glandular and luminal epithelial regions containing epithelial cells to discriminate between stromal and epithelial cells. Detection of UNK and stromal cells, and localisation of luminal epithelium from tissue boundaries was

addressed in Li et al. (2014). However, in Li et al. (2014) epithelial regions were discarded manually and it does not perform automatic segmentation of glandular epithelium and luminal epithelium to discard the epithelial cells.

In this paper, we propose novel cell orientation congruence descriptors for simultaneously segmenting both glandular epithelium and luminal epithelium (examples are shown in Fig. 1 (a) and (b)) from tissue boundaries in histology images of endometrial biopsy samples. A major difference between glandular epithelium and luminal epithelium is that the glandular epithelium encloses lumen inside the epithelial boundaries whereas luminal epithelium is usually at the edge. We observe that epithelial cells are arranged in a locally and neatly oriented manner as shown in Fig. 2. The distribution shows that the epithelial cells are oriented mainly in the similar direction as the difference from median is near zero except for a few neighbours for which the difference is in the range between $0-30^{\circ}$ due to curvature of the epithelium ($\Delta\theta = 4.98 \pm 5.51$). For non-epithelial cells, the difference from median is spread across the histogram due to irregular orientations of the stromal cells ($\Delta\theta = 37.77 \pm 35.29$). Based on this observation, we propose to use orientation of epithelial cells to extract a novel cell orientation congruence descriptor, by employing the orientation congruence in the neighbourhood of a cell. The strength of the proposed descriptors over the existing methods is that they are not restricted to segmentation of glandular epithelium with close boundaries, but are also capable of accurately segmenting disconnected (broken or open) glandular epithelium and luminal epithelium from the tissue boundaries. This paper is an extension of our previous work (Li et al. (2015))with the following additional novel contributions:

1. Introduction of the Multi-Ring Cell Orientation Congruence (MR-COCo) descriptor.
2. Validation of the proposed method on a larger data set, 150 visual fields compared to 30 visual fields in the conference publication.
3. Detailed experimentation on the choice of cellular neighbourhood, computational speed.

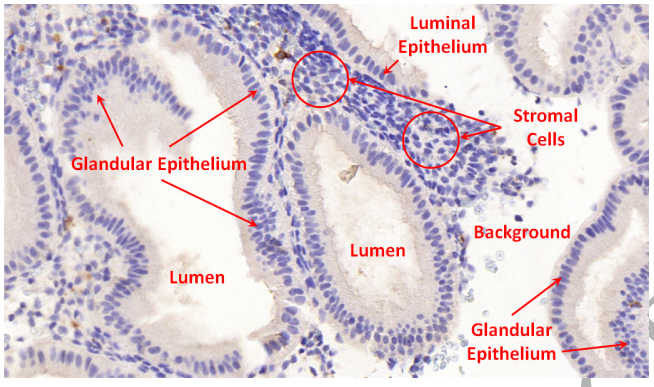

(a)

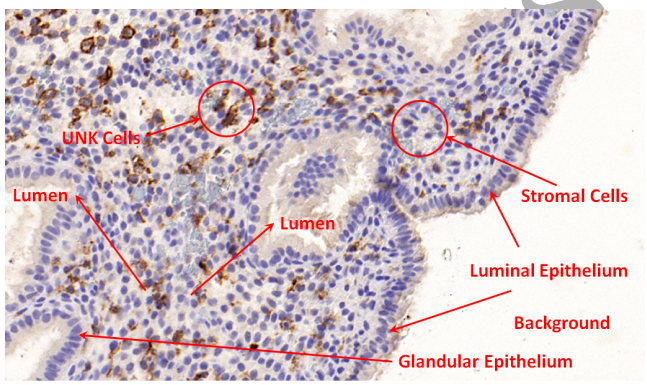

(b)

Figure 1: (a) and (b) are two example images of glandular epithelium and luminal epithelium.

4. Detailed critique on challenges faced by automated algorithms in segmentation of epithelial regions in endometrial biopsies.

The remainder of this paper is organised as follows. Related Work is summarised in Section 2. Image acquisition is described in Section 3. The preprocessing, i.e., cell detection and lumen segmentation, which are prerequisites for computing the proposed descriptors and epithelial cell classification, are explained in Section 4.1. We present the proposed descriptors in Sections 4.3. In Section 4.5, we show how to use epithelial cells classified by the proposed

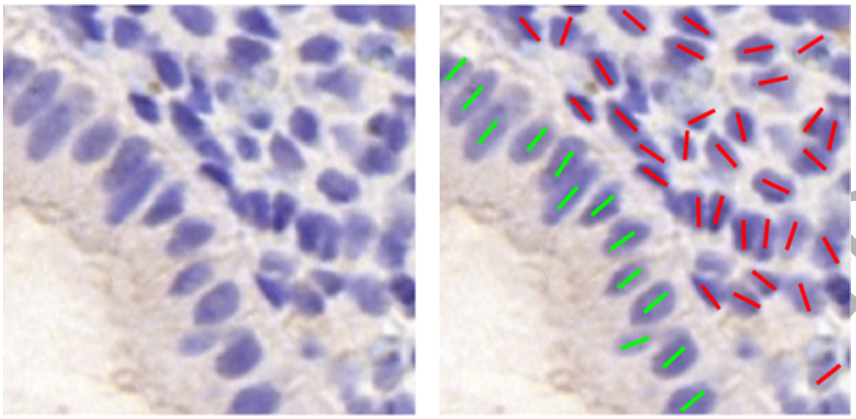

(a) (b)

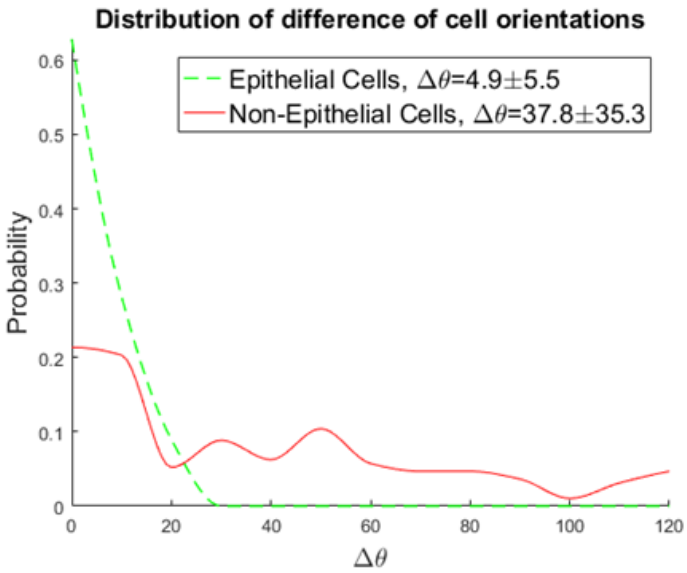

(c)

Figure 2: (a) Sample image cropped from a visual field from endometrial slide. (b) Orientations of epithelial cells overlaid in green and non-epithelial cells in red. (c) Distribution of difference of orientations of epithelial/non-epithelial cells from the median of all the orientations of epithelial/non-epithelial cells in green/red. It can be seen that neighbouring epithelial cells tend to have similar orientations.

descriptors with superpixels to achieve the final epithelium segmentation. Experimental results are presented and discussed in Section 5. Finally, the paper concludes with some directions for future work.

2. Related Work

To the best of our knowledge, there is no existing method on automatic segmentation of epithelium, both glandular and luminal, in endometrial biopsies. However, different methods have been proposed in literature for segmentation of glandular epithelial regions on other types of tissues. Glandular epithelium can be indirectly obtained by extracting it from glandular structures in most cases but it is difficult to extract luminal epithelium. Existing methods in literature are mainly based on employing two types of features: cell colour/texture and structural information of gland. Farjam et al. (2007) propose a variance filter which produces different texture features on lumen and cell regions and the segmentation is accomplished by clustering the texture features. Their method can be used for segmenting lumen or background regions. However, it is unable to differentiate between stromal and epithelial cell regions due to strong similarity of their textural features. Naik et al. (2008) use a Bayesian classifier to detect potential lumen regions and then initialise a level set curve on the boundaries of detected luminal area to finalise the segmentation. One limitation of this method is that its level set curve has difficulty with approximating epithelial boundaries with complex shape and texture. Nguyen et al. (2012) first label nuclei, cytoplasm and lumen by colour space analysis and utilise the constitution of glandular components to achieve the segmentation. Gunduz-Demir et al. (2010) construct an object graph of a set of circular objects decomposed from the image to identify the lumen. Then cell objects are used to form the boundary of glandular structures. Recently, Sirinukunwattana et al. (2015) proposed a novel Random Polygons Model (RPM) using epithelial cells as the vertices of a polygon to approximate boundaries of glands at the cost of relatively high computational complexity. A major limitation of such structure-based meth-

ods is that they rely on prior knowledge of the glandular structures. Lee et al. (2013) proposed a Cell Orientation Entropy (COrE) method which attempts to first qualitatively model cells/nuclei orientations by performing PCA on the cells/nuclei boundaries segmented using active contour, and then it quantifies the cell disorders by calculating the second order statistics for cell orientation from a co-occurrence matrix. This method can be potentially used for distinguishing differences between orientations of neighbouring epithelial and stromal cells/nuclei. Recently, Deep Learning (DL) techniques have been shown to produce promising results on gland segmentation Chen et al. (2016); Ronneberger et al. (2015) but DL approaches require a lot of training data and therefore we will focus on non-DL methods in this paper.

In endometrial histology, insignificant distinctive features, between epithelial cells and stromal cells, and also between lumen and background regions are observed, in terms of colour and morphology. Consequently, existing solutions listed above based on colour or texture features and composition of glandular structures may fail to segment epithelial cells correctly.

3. Materials

Endometrial biopsies were collected in a clinic at the University Hospitals Coventry and Warwickshire NHS Trust from patients suffering from recurrent pregnancy loss or recurrent IVF treatment failure. Written informed consent was obtained prior to tissue collection. The biopsies were taken in the mid-luteal phase and obtained using a Wallach Endocell sampler (Wallach, USA). The tissue was fixed in 10 formalin and embedded in paraffin wax. Sections (3μm) were labelled with anti-CD56 monoclonal antibody and stained with DAB and haematoxylin as per standard protocols in the pathology laboratory at the hospital. Stained tissue sections were scanned using Mirax Midi (Zeiss, Germany) at 0.25μm/pixel. Scans were assessed using Panoramic Viewer to identify regions for analysis. Digitised images were captured for each slide at 40$\times$ resolution and saved in the JPEG format. Images in the dataset used for

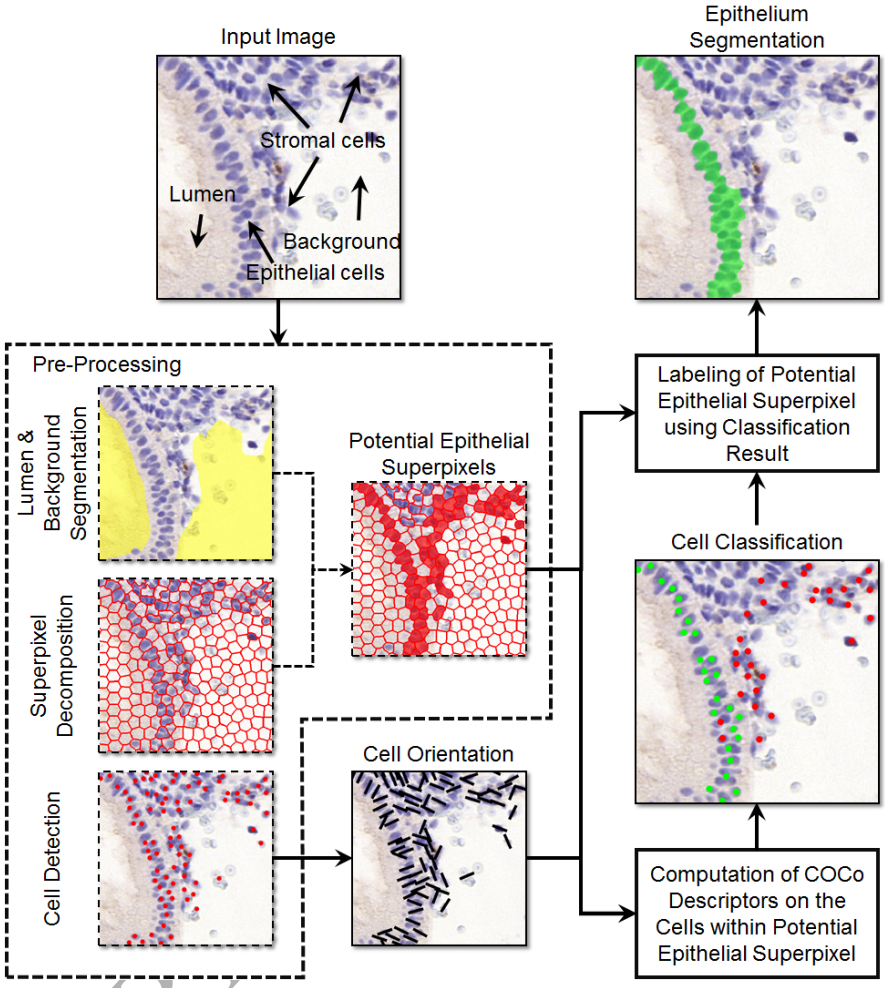

Figure 3: A block diagram of the proposed method with intermediate results of each step. Lumen segmentation is shown in transparent yellow, red grid marks superpixels, potential epithelial superpixels are shown in transparent red, red dots depict detected cells, black bars represent cell orientation, green dots depict epithelial cells classification using the proposed descriptors, and epithelial segmentation is shown in green.

experiment and evaluation of the proposed method are cropped regions in the high power fields (HPFs).

4. The Proposed Method

An overview of the proposed epithelial segmentation method is given by the block diagram in Fig. 3, which shows a workflow with the intermediate result of each main step. In the proposed method, we first perform a pre-processing step which detect cells and segments lumen or background regions to locate the superpixels of potential epithelium. Next, we compute the proposed descriptors for individual cells within these potential epithelial superpixels, and classify them into either epithelial or stromal cells by Random Forest classifier. Finally, potential epithelial superpixels containing classified epithelial cells are joined together to yield the segmentation of epithelial region.

4.1. Pre-processing

The input image is separated into the two underlying stain channels, Haematoxylin and DAB (CD56), using a colour deconvolution method proposed in Khan et al. (2014). The Haematoxylin channel is used for cell detection, lumen segmentation, and superpixel decomposition. We segment lumen and background of the input image using the variance filter in Farjam et al. (2007). It is based on the observation that lumen or background are large homogeneous regions with small local standard deviations, while regions with dense cellular populations are the opposite. We denote a set of pixels segmented as lumen or background as Seg_{lb}. We decompose the input image into superpixels using the Simple Linear Iterative Clustering (SLIC) algorithm proposed by Achanta et al. (2012). A superpixel denoted as P is a set of pixels, that depict a small homogeneous region depicting either lumen, background or cell in our cases. We classify superpixels into two categories: lumen and cell superpixels. A superpixel P is a lumen superpixel and denoted as S_l depicting a lumen region if $|Seg_{lb} \cap P| \geq \frac{1}{2}|P|$, $|...|$ represents cardinality of a set. Otherwise it is a cell superpixel and denoted as S_c, which depicts either an epithelial or a stromal cell region. An S_c is defined as $1st$ level *potential* epithelial superpixel (S_e^1) if it immediately connects to any S_l. Similarly, an S_c is defined as a $2nd$ level

potential epithelial superpixel (S_e^2) if it immediately connects to any S_e^1 but not to S_l. We merge both S_e^1 and S_e^2 to yield the *potential* epithelium regions. This is because an epithelium can be formed by multiple layers of epithelial cells, thus we also define some superpixels which are more distant to lumen regions as *potential* epithelial superpixels.

It is important to mention that localisation of the cell positions is prerequisite to compute the proposed descriptors, though cell segmentation is not necessary. We detect cells using an extended version Li et al. (2014) of Local Isotropic Phase Symmetry Measure (LIPSyM) method proposed in Kuse et al. (2011). The method is based on the assumption that stromal and epithelial nuclei appear as elliptical blobs where the pixels near to their centers show peaks of local symmetry.

4.2. Estimation of cell orientations

In this step, the Haematoxylin channel is used as a gray-scale input image which is normalised to zero mean and unit variance in order to reduce the variations in pixel value of cell and background regions from different images, which facilitates the subsequent image processing steps (Hong et al. (1998)). After normalisation, we calculate pixel-level orientation $O_p(i,j)$ at pixel (i,j) of the input image with the help of gradient direction (Gonzalez and Woods (2008)).

We then estimate the orientation of a cell 'c' using the pixel-level orientations at a set of its neighbouring pixels within a circular pixel neighbourhood $\mathcal{N}_p(c)$ defined as,

$$\mathcal{N}_p(c) = \left\{ p \in Mask^h | dist(c,p) \leq r \right\} \tag{1}$$

where p is a pixel from the input image, $Mask^h$ is a binary mask image segmented from the Haematoxylin channel using Otsu Thresholding (Otsu (1975)), $dist(c,p)$ is the Euclidean distance between p and the center of c, and r is a scalar in pixel value which defines the radius of $\mathcal{N}_p(c)$. In our cases, we empirically chose r to be 7 pixels, which was found to roughly cover a cell nucleus. Fig. 4(a) shows the estimated pixel orientations.

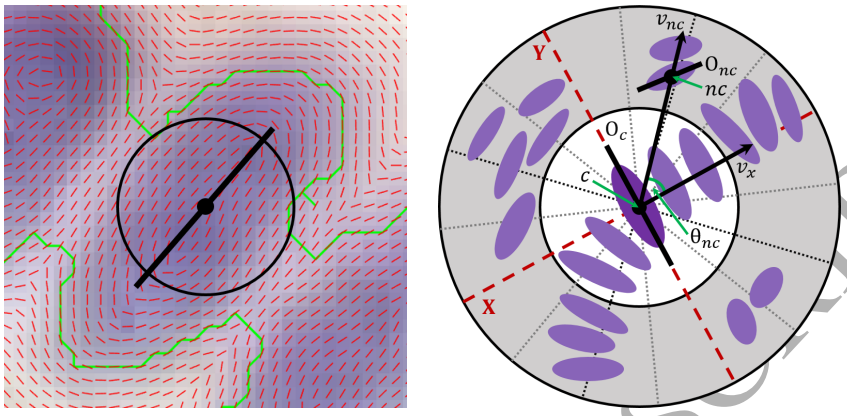

(a) (b)

Figure 4: (a) shows the cell orientation estimation of a cell, the black circle is the pixel neighbourhood used for sampling neighbouring pixels of the cell, the binary mask (cell segmentation) of Haematoxylin is shown in green, red bars depict pixel orientations and the black line depicts the orientation of a cell; (b) shows illustration of the COCo descriptor for a detected cell. Black dots depict the positions of the detected cell, purple shapes depict cells, black circles mark the cell neighbourhoods of the descriptors, black dashed lines divide the angular sections of the cell neighbourhoods, red dashed lines are coordinate axes, the"ring-like" cell neighbourhoods of the descriptors are shown in gray, black lines depict the cell orientation and black arrows depict vectors.

To estimate the orientation of the cell c, we first define a pixel orientation histogram $\mathcal{H}(c)$ for $\mathcal{N}(c)$ as,

$$\mathcal{H}(c) = \{h_1, h_2, ..., h_7\} \tag{2}$$

The count h_k for the kth bin is calculated as follows:

$$\begin{aligned} h_k &= \sum_{p=1}^{|\mathcal{N}(c)|} C(O_p, k), \ k = 1, 2, ..., 7 \\ C(O_p, k) &= \begin{cases} 1, & if \ \frac{(k-1)\pi}{8} \leq O_p \leq \frac{(k+1)\pi}{8} \\ 0, & otherwise \end{cases} \end{aligned} \tag{3}$$

where $C(O_p, k)$ is an indicator function that indicates to which bin the orien-

tation of a pixel p belongs. We then estimate the orientation denoted as O_c of cell c using the largest bin of $\mathcal{H}(c)$ as follows,

$$O_c = \frac{1}{h_l} \sum_{p=1}^{|\mathcal{N}(c)|} O_p \cdot C(O_p, l)$$
$$l = \arg\max\big(\mathcal{H}(c)\big) \tag{4}$$
$$h_l = \max\big(\mathcal{H}(c)\big)$$

Fig. 4(a) shows the cell orientation estimation of a cell.

4.3. Computation of the Cell Orientation Congruence (COCo) descriptor

To compute the COCo descriptor for a cell c, we first define a circular cell neighbourhood denoted as $\mathcal{N}_c(c)$ for c, which is shown in Fig. 4(b) and given as:

$$\mathcal{N}_c(c) = \big\{nc | dist(c, nc) \leq d\big\} \tag{5}$$

where nc is a neighbouring cell within distance d, $dist(c, nc)$ denotes the Euclidean distance between the centers of c and nc, and d is the radius of $\mathcal{N}_c(c)$. The circular cell neighbourhood $\mathcal{N}_c(c)$ is divided into a set of 16 half-overlapping (with overlap of $\frac{\pi}{8}$) angular sections with the same angular width of $\frac{\pi}{4}$. We experimentally found that 16 bins were enough to cover all the neighbouring cell orientations and choosing more than 16 was redundant. The division of angular sections starts clockwise from the Y-axis which is aligned with the orientation of c. The division is illustrated in Fig. 4(b).

We then calculate the cell orientation congruence Co_n of the nth angular section of $\mathcal{N}_c(c)$ using orientation of the cells located in angular section as follows:

$$Co_n = \sum_{nc=1}^{|\mathcal{N}_c(c)|} \Omega_{nc} \cdot \cos(\Phi_{nc}) \cdot I(\Delta_{nc}, n),$$
$$n = 1, 2, ..., 16 \tag{6}$$

where

$$\Omega_{nc} = \frac{\omega_{nc}}{\sum_{nc=1}^{|N_c(c)|} \omega_{nc}}, \quad \omega_{nc} = e^{\frac{-D_{nc}^2}{2\sigma^2}}$$

$$\Phi_{nc} = \begin{cases} \pi - |O_c - O_{nc}|, & if\ |O_c - O_{nc}| \geq \frac{\pi}{2}, \\ |O_c - O_{nc}|, & otherwise \end{cases}$$

$$I(\Delta_{nc}, n) = \begin{cases} 1, & if\ \frac{(n-1)\pi}{8} \leq \Delta_{nc} \leq \frac{(n+1)\pi}{8} \\ 0, & otherwise \end{cases}$$

$$\Delta_{nc} = \begin{cases} 2\pi - |\Theta_{nc} - O_c|, & if\ \Theta_{nc} - O_c \leq 0, \\ \Theta_{nc} - O_c, & otherwise \end{cases}$$

$$\Theta_{nc} = \begin{cases} 2\pi - |\theta_{nc}|, & if\ \theta_{nc} < 0, \\ \theta_{nc}, & otherwise \end{cases}$$

$$\theta_{nc} = \arccos\left(\frac{v_{nc} \cdot v_x}{||v_{nc} \cdot v_x||}\right)$$

In the above equations, Ω_{nc} is the weight given to nc, which is calculated based on its Euclidean distance D_{nc} to the center of c using a standard deviation σ, Φ_{nc} is the orientation difference of nc compared with c, $I(\Delta_{nc}, n)$ is an indicator function that indicates whether nc is located in the nth angular section of $\mathcal{N}_c(c)$, v_{nc} is a vector from the center of c to the center of nc, v_x is an unit vector along the x-axis, and θ_{nc} is the angle between v_{nc} and v_x. Fig. 4 (b) illustrates how to localise a nc for an angular section of the COCo descriptor and compute the cell orientation congruence of this angular section.

We finally express the COCo descriptor of the cell c as a feature vector $COCo(c)$ consisting of the cell orientation congruences of 16 angular sections as:

$$COCo(c) = \langle Co_1, Co_2, ..., Co_{16} \rangle \tag{7}$$

The above descriptor calculated for the epithelial cell c shown in Fig. 4(b) is likely to have relatively large values in the first element Co_1 and middle element Co_{10}, which tend to exhibit the orientation congruence of its cell neighbourhood.

4.4. Multi-Ring COCo Descriptor

The COCo descriptor is designed to capture differences in orientations of cells in a neighbourhood. A limitation of the single-radius version of COCo descriptor is that it is susceptible to noisy cell orientations in the vicinity of a cell. We propose a multi-ring construction of our descriptor, which not only helps to include features from larger neighbourhoods but also filters the descriptor for orientations from noisy regions such as those containing clumped cells. We define a "ring-like" cell neighbourhood (shown in gray colour in Fig. 4(a) and (b)) of the epithelial cell c as:

$$\mathcal{R}_i(c) = \left\{ nc | d_{inner} \leq dist(c, nc) \leq d_{outer} \right\} \tag{8}$$

where nc is a neighbouring cell in $\mathcal{R}_i(c)$, d_{inner} and d_{outer} are inner and outer radii respectively.

Given a set of COCo descriptors computed using different sizes of "ring-like" cell neighbourhoods of the cell c, the multi-ring version of the COCo descriptor of the cell c, which we term here as the Multi-Ring Cell Orientation Congruence (MR-COCo) descriptor, is given as a feature vector $MRCOCo(c)$ which concatenates the set of COCo descriptors,

$$\begin{aligned} &MRCOCo(c) \\ &= \left\langle COCo(c)_1, COCo(c)_2, ..., COCo(c)_{nrings} \right\rangle \end{aligned} \tag{9}$$

where $nrings$ denotes the number of rings and $COCo(c)_i$ is calculated using $\mathcal{R}_i(c)$ as defined above in (8) instead of $\mathcal{N}_c c$ as in (5). The MR-COCo descriptor can more comprehensively describe the cell orientation congruence by considering a diversity of cell neighbourhoods of a cell.

4.5. Epithelium segmentation by labelling potential epithelium superpixels

For epithelium segmentation, we first compute the proposed descriptors from both epithelial and non-epithelial cells located within potential epithelial superpixels as described above. Secondly, we employ the random forests classifier (Breiman (1996, 2001); Breiman and Cutler) with the proposed descriptors to

identify epithelial cells. Next, a potential epithelial superpixel which contains any non-epithelial cells or no cells is initially categorised as a non-epithelial superpixel, S_{ne}, otherwise it is marked as an epithelial superpixel, S_{pe}. In the former case i.e., superpixels with a few non-epithelial cells, superpixels may be mistakenly classified as non-epithelial. Therefore, we perform a refinement process to re-classify these non-epithelial superpixels, S_{ne}, as described below:

1. Given S_{ne}, we define a S_{pe} which immediately connects to S_{ne} as its level 1 neighbour denoted as S_i^1. A set of S_i^1 is denoted as $\{S_i^1\}$;
2. We define a S_{pe} as a level 2 neighbour of S_{ne} if it immediately connects to any S_i^1 and $S_{pe} \notin \{S_j^1\}$, denoted as S_j^2. The set of level 2 neighbours is denoted as $\{S_j^2\}$;
3. Cells identified as epithelial cells by the random forests classifier with the proposed descriptors are defined as true epithelial cells, otherwise they are defined as false epithelial cells. The numbers of true and false epithelial cells within S_{ne} and its neighbours $\{S_i^1\}$ and $\{S_j^2\}$ are counted and denoted as N_{true} and N_{false}, respectively. S_{ne} is remarked as an epithelial superpixel if $N_{true} \geq N_{false}$, otherwise it remains as a non-epithelial superpixel.

A binary image is segmented by joining all epithelial superpixels together after the refinement step. We then achieve the final epithelium segmentation by removing small isolated connected components from the binary image. We empirically chose to remove a region that has area smaller than 500 pixels.

5. Experimental Results

We devise three experiments with gradually increasing complexity in order to comprehensively evaluate the segmentation accuracies of the proposed descriptors. In addition, we performed three-fold cross validation. For each cross validation, we divided the data randomly into three subsets and chose two subsets for training and the remaining subset for testing.

The first experiment examines the segmentation accuracy of the proposed descriptors, i.e., COCo, MR-COCo on a randomly selected subset of the image dataset. In addition, their computational speeds are also evaluated using the same subset. The second experiment compares the proposed MR-COCo in the first experiment with five state-of-the-art methods, i.e., Farjam et al. (2007), Naik et al. (2008), Nguyen et al. (2012), Sirinukunwattana et al. (2015) and Lee et al. (2013). To the best of our knowledge there is no existing method on segmentation of both glandular & luminal epithelium in literature. However, the above five methods are proposed mainly for segmenting glands rather than luminal epithelium, this experiment aims to evaluate the performance of the proposed descriptors against the other methods on segmenting glandular epithelium. Our image dataset contains 150 images. The images were initially annotated by one expert to obtain the ground truth markings and then verified by a second more senior expert. As the other methods we compare with are designed for segmentation of glands, we perform two set of experiments to make the comparison fair. We first manually select a subset (50 images) from the image dataset to guarantee that each image contains at least one glandular structure. Next, we manually crop a sub-image from each of these images, which contain only glandular structures. The sub-images are then used in the experiment in Section 5.2 where we only compare the performance of different methods on segmentation of glandular structures. To highlight the advantages of the proposed method, we compare MR-COCo with all the state-of-the-art methods in Section 5.3 where we use all the data set (150 images). The images of this dataset may contain either or both of the luminal and glandular epithelium.

We evaluate the segmentation accuracy using a modified version of the Dice-score inspired by Sirinukunwattana et al. (2015) in pixel-level and epithelium-level. The closer to 1 the Dice score, the more accurate is the segmentation. The pixel-level Dice score is calculated as:

$$Dice_{pix}(Seg, Grt) = 2\left(\frac{|Seg \cap Grt|}{|Seg| + |Grt|}\right) \tag{10}$$

where $Dice_{pix}$ is the pixel-level Dice score, Seg is the set of pixels segmented as an epithelium and Grt is the set of pixels annotated as the ground truth. We consider all segmented epithelium in an image as a whole for calculating pixel-level Dice score.

To measure the weighted accuracy of segmenting individual epithelium, we calculate the epithelium-level Dice score based on the pixel-level Dice score as follows,

$$\begin{gathered} Dice_{epi}(Seg, Grt) = \\ \frac{1}{2}\left(\sum_{i=1}^{NS} w_i \cdot Dice_{pix}(Seg_i, Grt_i) + \sum_{i=1}^{NG} \dot{w}_i \cdot Dice_{pix}(\dot{Grt}_i, \dot{Seg}_i)\right) \\ w_i = \frac{1}{2}\left(\frac{|Seg_i|}{|Seg|} + \frac{|Grt_i|}{|Grt|}\right) \\ \dot{w}_i = \frac{1}{2}\left(\frac{|\dot{Grt}_i|}{|Grt|} + \frac{|\dot{Seg}_i|}{|Seg|}\right) \end{gathered} \tag{11}$$

where $Dice_{obj}$ is the object-level Dice score, Seg_i is a set of pixels segmented as the ith epithelium region in the image, Grt_i is a set of pixels annotated as the ith ground truth region which maximally overlaps with Seg_i among all ground truth regions in the image, NS is the total number of the segmented epithelium regions in the image, $\dot{Grt}_i$ is a set of pixels segmented as the ith ground truth region in the image, $\dot{Seg}_i$ is a set of pixels segmented as the ith epithelium region which maximally overlaps with Seg_i among all segmented epithelium regions in the image, and NG is the total number of ground truth regions in the image.

5.1. Comparison of the proposed descriptors for epithelium segmentation

The radius (in pixels) of the neighbourhood is a sensitive and key parameter in all of the proposed descriptors. The radius size is empirically tuned based on the image dataset. This experiment examines the performance of different radii for the proposed descriptors, and also compares the accuracy of these descriptors for both luminal and glandular epithelium segmentation. The idea of the proposed descriptors is to take the advantage of orientation congruence of neighbouring cells. The radius and neighbourhood size are proportional to the

average size of cells in terms of pixels in the image. The radius should be large enough to guarantee that the descriptors can locate a sufficient number of cells within the defined neighbourhood. We set the radius initially to 60 pixels to allow the proposed descriptors to capture a couple of cells, and then increase it by 30 pixels up to a maximum of 180 pixels. We empirically chose 3 "ring-like" neighbourhoods for the multi-ring version of the proposed descriptors.

Fig. 5 shows the segmentation accuracy of the proposed descriptors with different neighbourhood radii in terms of average dice scores. The results show that the proposed descriptors performed poorly with a radius of 60 pixels. The proposed multi-ring descriptor have much lower accuracy compared with the cell descriptors using a single neighbourhood. This is due to fact that a small radius does not allow locating enough cells to compute the orientation congruence, especially, very few of cells can be found within a ring of 20 pixels, 60/3, in the multi-ring version. The accuracy of the proposed descriptors is significantly improved by increasing radius but decreases when their radii becomes larger than 120 pixels. The MR-COCo outperforms the COCo descriptor in terms of the average Dice score. In conclusion, the multi-ring neighbourhood improves the accuracy of the proposed descriptors with an appropriate value for the radius as shown in Fig. 5.

The average computational speeds per image (for average 975.4 detected cells per image) of the proposed descriptors are given in Fig. 6. All the results were generated using Matlab 2015b running on a Windows 10 machine with 2.5GHz Intel Xeon E5-2760 v2 processor and 64GB RAM. The computational costs of these descriptors increase as the neighbourhood radius increase. The cost of the MR-COCo descriptor is roughly 3 times of the COCo descriptor. This is due to the fact that 3 ring-like neighbourhoods are used for the MR-COCo descriptor in the experiment, which can be considered as repeating 3 times the computations of the COCo descriptor. This can be optimised by parallelising the computation.

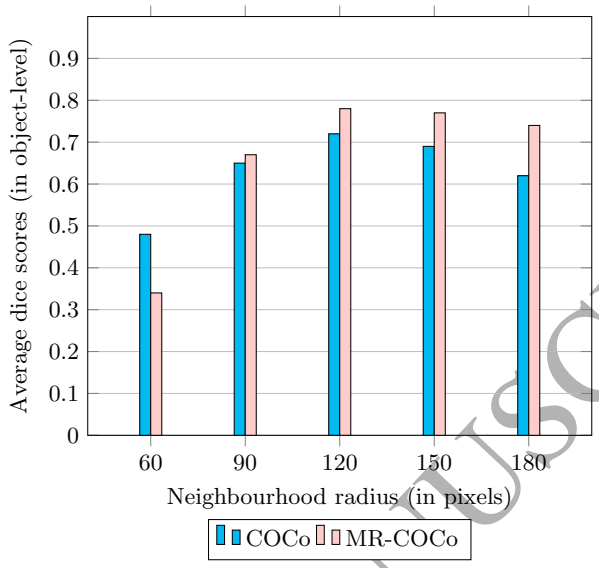

Figure 5: Epithelium segmentation object dice scores of the proposed descriptors.

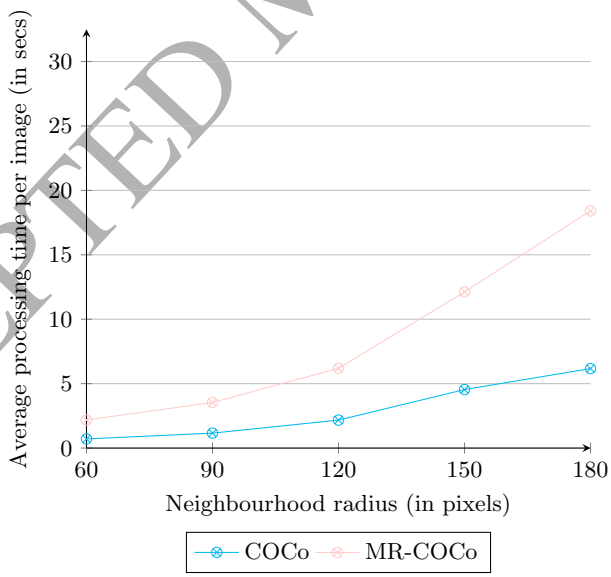

Figure 6: Computational speeds of the proposed descriptors.

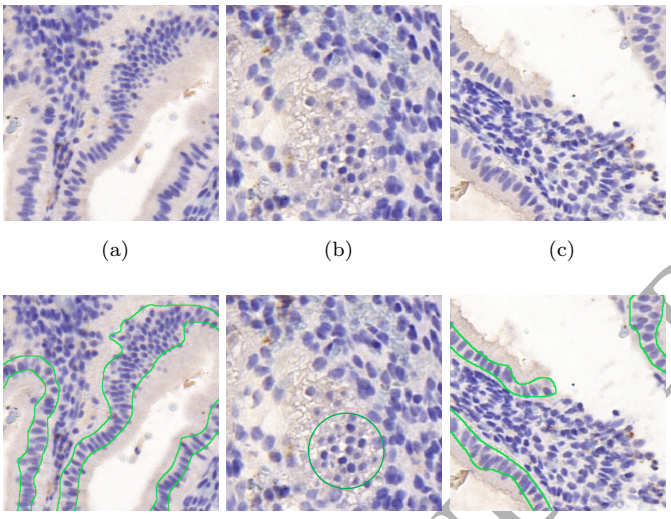

Figure 7: (a), (b) and (c) are three sample images whereas the ground truth for epithelium is manually marked using green lines in (d) and (f). The green line in (e) marks "hive-like' cluster of epithelial cells.

5.2. Evaluation of MR-COCo descriptors for glandular epithelium segmentation

In this experiment, the MR-COCo descriptor is evaluated against Farjam et al. (2007), Naik et al. (2008), Nguyen et al. (2012), Sirinukunwattana et al. (2015), and Lee et al. (2013) for segmenting glands on 50 sub-images which contain only glandular structures. The algorithms in Farjam et al. (2007) Naik et al. (2008), Nguyen et al. (2012), and Sirinukunwattana et al. (2015) were proposed for segmenting complete glandular structure but as mentioned above, to the best of our knowledge there is no existing literature on segmentation of both luminal and glandular epithelial regions in endometrial biopsies. The methods mentioned above generally connect a set of epithelial cells to generate a close boundary that marks the glandular structures. To make the comparison fair for the task of epithelium segmentation, in their results we morphologically dilate these boundaries by the average thickness (30 pixel) of glandular epithelium, and also remove lumen regions from segmented glandular structures, in order

to achieve the segmentation of epithelium by these methods.

The results of the comparison are reported in Table 1 which show that MR-COCo descriptor yields top accuracy among all the compared methods. In reality, thickness of epithelium can differ greatly between different glandular structures and even within one glandular structure as shown in Fig. 7(a). Therefore, the proposed descriptors achieve better accuracy than other methods which try to construct a boundary of glandular structures using a single layer of epithelial cells. An image with varied thickness of glandular epithelium is shown in Fig. 7(a), and the segmentation results in Fig. 8(j) show that accurate segmentation of glandular epithelium of variable thickness can be simultaneously achieved when using the MR-COCo descriptor. Another common problem of these methods is that large blank regions between cell clusters are often mistakenly segmented as lumen by them. Both Fig. 7(a) and 7(b) show examples of a such cases. In the top-middle of Fig. 7(a), we observe that an elongated blank region is surrounded by stromal cells on the left side and epithelium on the right side. In Fig. 7(c), a large blank region at the centre is enclosed by stromal cells. Our method first labels the blank region as lumen and its surrounding cell regions as potential epithelium regions. Next, the cells within these regions are classified using the proposed descriptors. In Fig. 7(a), the stromal cell region is completely removed from the segmentation result. Although a few of cells are mistakenly classified as epithelial cells from Fig. 7(c) in Fig. 8(l), most of the potential epithelium regions are also finally removed since a majority of cells within these regions are stromal cells. On the other hand, the other methods generally consider blank region as lumen and then construct a boundary surrounding this blank region to report a glandular structure. In addition, Nguyen et al. (2012) uses a colour-based pixel clustering method to classify stromal and epithelial cell. This causes the stromal and epithelial cells to be segmented as one cell type. Thus the segmentation result of Nguyen et al. (2012) is also affected by incorrect epithelial cell classification. The active contour based cell segmentation method in Lee et al. (2013) has difficulty in segmenting dense cell cluster as separate individual cells. Consequently their PCA based cell orien-

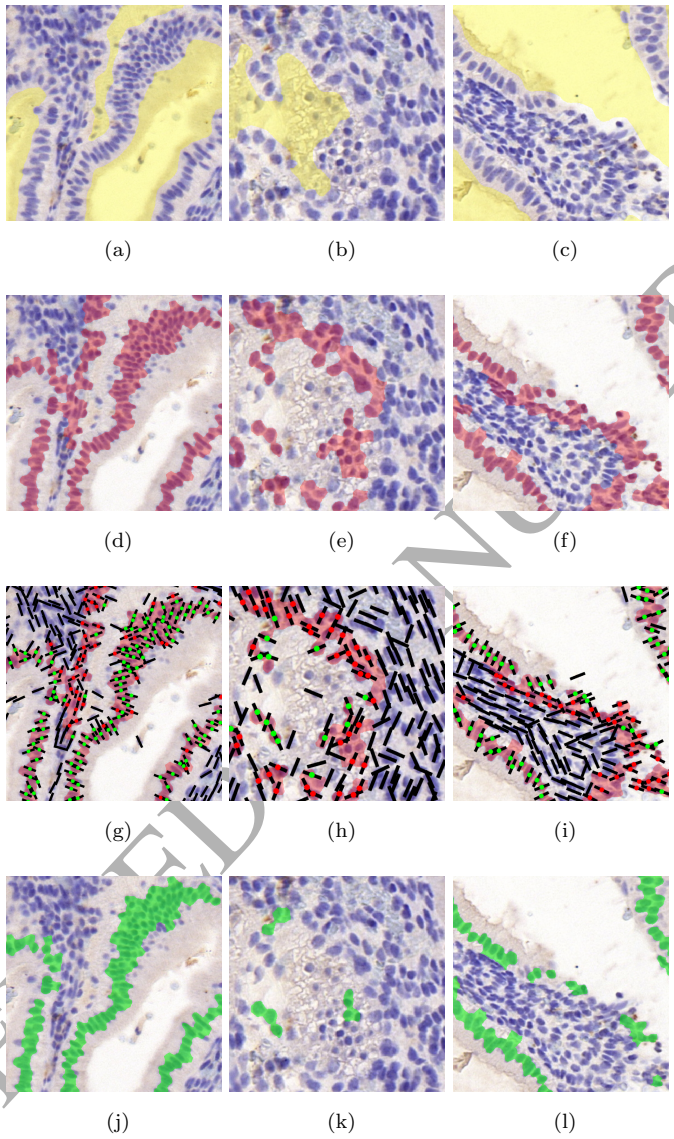

Figure 8: Lumen segmentation for the sample images in Figure 7 are shown in transparent yellow in (a), (b) and (c), potential epithelium region is shown in transparent red in (d), (e) and (f); (g), (h) and (i) are classification images of Figure 7 (a), (b) and (c) using the MR-COCo descriptor, in which black bars depict cell orientations, red dots non-epithelial cells and green dots depict epithelial cells within potential epithelium regions; epithelium segmentation results are shown in transparent green in (j), (k) and (l) in the last row.

tation estimation method fails. Thus the problems of cell segmentation cause Nguyen et al. (2012) and Lee et al. (2013) to perform poorly on the images with large blank stromal regions due to relatively sparse distribution of cells and densely grouped cells. So Nguyen et al. (2012) and Lee et al. (2013) attain low accuracy, and also large standard deviations are reported in their Dice score.

We observe a small "hive-like" epithelial structure which is marked by a green circle at the bottom of the truth image in Fig. 7(e). Both the proposed descriptors and all the state-of-the-art methods are not able to detect this structure due to the fact that no lumen region can be found in the first place to locate it. Another problem of the proposed descriptors is that the cell orientation estimation of the cells from "hive-like" epithelial structures is inaccurate due to their small circular shapes. Moreover, their cell orientation congruence is similar to some of the stromal cells. Hence, the "hive-like" epithelial structure becomes the main challenge preventing our method from generating very accurate segmentation results.

Table 1: Segmentation accuracy of the proposed descriptor compared to different methods on sub-images containing only glandular epithelium. Dice scores are reported by the averages ± standard deviations and the best results are in bold.

Methods	Dice Scores	
	Pixel-Level	Epithelium-Level
Nguyen et al. (2012)	0.61 ± 0.08	0.59 ± 0.08
COrE Lee et al. (2013)	0.65 ± 0.08	0.62 ± 0.09
Naik et al. (2008)	0.72 ± 0.04	0.71 ± 0.05
Farjam et al. (2007)	0.76 ± 0.04	0.74 ± 0.05
TGPM Sirinukunwattana et al. (2015)	0.75 ± 0.03	0.74 ± 0.03
MR-COCo	$\mathbf{0.79 \pm 0.03}$	$\mathbf{0.78 \pm 0.03}$

5.3. Evaluation of the MR-COCo descriptor for glandular and luminal epithelium segmentation

Table 2 indicates that the state-of-the-art methods perform with a lower accuracy in this experiment. The MR-COCo descriptor slightly dropped the accuracy by only 0.02, showing that it is also able to accurately segment luminal epithelium. The algorithms in Farjam et al. (2007), Naik et al. (2008), Nguyen et al. (2012), and Sirinukunwattana et al. (2015) produce lower accuracy than in the above experiment because lumen segmentation used in these methods cause the background regions to be also segmented as lumen due to their high similarity in our dataset. Consequently, the stromal cells at the boundary of background regions are mistaken for epithelial cells, since they have similar texture, colour and shape features to their neighbouring epithelial cells. Fig. 7(c) shows an example of such a case. A large empty background region is normally segmented as lumen and then all nearby cells are used to generate a boundary which is segmented as a glandular structure by the other methods. In fact, the ground truth image in Fig. 7(f) shows that only the cells at the top-left and the bottom-right of the background are from luminal epithelium, despite the fact that they are located at the same diagonal edge which is a background boundary. In the results, the classification of these cells is performed accurately by using the MR-COCo descriptor.

In addition, all the state-of-the-art methods assume a closed boundary for the glandular epithelium. But luminal epithelium regions are normally curves or lines and do no belong to any glandular structure, as shown in Fig. 7(a). The algorithm in Lee et al. (2013) produces a low accuracy due to the fact that the cells at luminal epithelium are more frequently overlapped or in dense cluster, which makes the cell segmentation even more challenging for their active contour based method.

In summary, the experimental results show that the MR-COCo descriptor is relatively robust for segmentation of luminal epithelium and all the state-of-the-art methods have poor performance on segmenting luminal epithelium.

Table 2: Segmentation accuracies of the proposed descriptor and all the state-of-the-art methods on the completed image dataset for both glandular and luminal epithelium. Dice scores are reported by the averages ± standard deviations and the best results are in bold.

Methods	Dice Scores	
	Pixel-Level	Epithelium-Level
Nguyen et al. (2012)	0.58 ± 0.09	0.56 ± 0.10
COrE Lee et al. (2013)	0.58 ± 0.11	0.54 ± 0.12
Naik et al. (2008)	0.66 ± 0.05	0.65 ± 0.05
Farjam et al. (2007)	0.67 ± 0.05	0.66 ± 0.06
TGPM Sirinukunwattana et al. (2015)	0.70 ± 0.04	0.68 ± 0.05
MR-COCo	$\mathbf{0.76 \pm 0.05}$	$\mathbf{0.76 \pm 0.05}$

6. Conclusions

In this paper, we presented cell orientation congruence descriptor and its multi-ring version which aim to solve the problem of simultaneously segmenting both luminal and glandular epithelium segmentation in endometrial histology images. The proposed descriptors are designated to discriminate between epithelial and stromal cells based on the observation that the epithelial cells in normal endometrium are depicted with an orientation that is similar to that of their neighbouring cells along certain directions whereas neighbouring stromal cells are packed depicted following an entirely different pattern. The results show that the MR-COCo descriptor yields the best results compared to COCo and to the 5 state-of-art methods in two experiments. The experimental results show that the MR-COCo descriptor attains a superior segmentation accuracy, particularly for simultaneously segmenting both luminal and glandular epithelium.

The COCo descriptor has been designed to segment epithelial regions (con-

sisting of both glandular epithelium and luminal epithelium) that generally contain cells exhibiting congruence in their orientation. The proposed descriptor can be adapted to segment epithelial regions in adenocarcinomas (cancers of the epithelial tissue, for example in breast, lung and colon) where neighbouring epithelial cells again exhibit cell orientation congruence, i.e. neighbouring epithelial cells have similar orientations. We believe that this gives the COCo descriptors wider applicability in the analysis of histology images of adenocarcinomatous tissue slides. We intend to validate the proposed descriptors on a much larger dataset of both cancer and non-cancer histology images consisting of epithelial regions. A potential direction of future research is to efficiently parallelise the computation of the proposed descriptors.

Acknowledgment

We are grateful to Prof Siobahn Quenby of the Warwick Medical School and her team for providing the dataset used in this work and handmarking the ground-truth segmentations. We are thankful to Dr Victor Sanchez for his feedback on an earlier version of this manuscript.

References

Achanta, R., Shaji, A., Smith, K., Lucchi, A., Fua, P., Susstrunk, S., 2012. Slic superpixels compared to state-of-the-art superpixel methods. Pattern Analysis and Machine Intelligence, IEEE Transactions on 34, 2274–2282.

Arif, M., Rajpoot, N., 2007. Classification of potential nuclei in histology images using shape manifold learning, in: Proceedings International Conference on Machine Vision (ICMV'2007).

Breiman, L., 1996. Bagging predictors. Machine learning 24, 123–140.

Breiman, L., 2001. Random forests. Machine learning 45, 5–32.

Breiman, L., Cutler, A., . Random Forests. `http://www.stat.berkeley.edu/~breiman/RandomForests/`.

Chen, H., Qi, X., et al., 2016. Dcan: Deep contour-aware networks for accurate gland segmentation. arXiv preprint arXiv:1604.02677 .

Farjam, R., Soltanian-Zadeh, H., Jafari-Khouzani, K., Zoroofi, R.A., 2007. An image analysis approach for automatic malignancy determination of prostate pathological images. Cytometry Part B: Clinical Cytometry 72, 227–240.

Gonzalez, R.C., Woods, R.E., 2008. Digital image processing. Nueva Jersey .

Gunduz-Demir, C., Kandemir, M., Tosun, A.B., Sokmensuer, C., 2010. Automatic segmentation of colon glands using object-graphs. Medical image analysis 14, 1–12.

Gurcan, M.N., Boucheron, L.E., Can, A., Madabhushi, A., Rajpoot, N.M., Yener, B., 2009. Histopathological image analysis: A review. Biomedical Engineering, IEEE Reviews in 2, 147–171.

Hong, L., Wan, Y., Jain, A., 1998. Fingerprint image enhancement: algorithm and performance evaluation. Pattern Analysis and Machine Intelligence, IEEE Transactions on 20, 777–789.

Khan, A.M., Rajpoot, N., et al., 2014. A non-linear mapping approach to stain normalisation in digital histopathology images using image-specific colour deconvolution. IEEE Transactions on Biomedical Engineering .

Kuse, M., Wang, Y.F., Kalasannavar, V., Khan, M., Rajpoot, N., 2011. Local isotropic phase symmetry measure for detection of beta cells and lymphocytes. Journal of pathology informatics 2.

Lee, G., Ali, S., Veltri, R., Epstein, J.I., Christudass, C., Madabhushi, A., 2013. Cell orientation entropy (core): Predicting biochemical recurrence from prostate cancer tissue microarrays, in: Medical Image Computing and Computer-Assisted Intervention–MICCAI 2013. Springer, pp. 396–403.

Li, G., Raza, S.E.A., Rajpoot, N., 2015. A novel cell orientation congruence descriptor for superpixel based epithelium segmentation in endometrial histol-

ogy images, in: International Workshop on Patch-based Techniques in Medical Imaging, Springer. pp. 172–179.

Li, G., Sanchez, V., Patel, G., Quenby, S., Rajpoot, N., 2014. Localisation of luminal epithelium edge in digital histopathology images of ihc stained slides of endometrial biopsies. Computerized Medical Imaging and Graphics .

Naik, S., Doyle, S., Agner, S., Madabhushi, A., Feldman, M., Tomaszewski, J., 2008. Automated gland and nuclei segmentation for grading of prostate and breast cancer histopathology, in: Biomedical Imaging: From Nano to Macro, 2008. ISBI 2008. 5th IEEE International Symposium on, IEEE. pp. 284–287.

Nguyen, K., Sarkar, A., Jain, A.K., 2012. Structure and context in prostatic gland segmentation and classification, in: Medical Image Computing and Computer-Assisted Intervention–MICCAI 2012. Springer, pp. 115–123.

Otsu, N., 1975. A threshold selection method from gray-level histograms. Automatica 11, 23–27.

Quenby, S., Nik, H., Innes, B., Lash, G., Turner, M., Drury, J., Bulmer, J., 2009. Uterine natural killer cells and angiogenesis in recurrent reproductive failure. Human reproduction 24, 45–54.

Ronneberger, O., Fischer, P., et al., 2015. U-net: Convolutional networks for biomedical image segmentation, in: International Conference on Medical Image Computing and Computer-Assisted Intervention, Springer. pp. 234–241.

Sirinukunwattana, K., Snead, D., Rajpoot, N., 2015. A stochastic polygons model for glandular structures in colon histology images. Medical Imaging, IEEE Transactions on .

Snead, D.R., Tsang, Y.W., Meskiri, A., Kimani, P.K., Crossman, R., Rajpoot, N.M., Blessing, E., Chen, K., Gopalakrishnan, K., Matthews, P., et al., 2015. Validation of digital pathology imaging for primary histopathological diagnosis. Histopathology .

505 Tang, A.W., Alfirevic, Z., Turner, M.A., Drury, J.A., Small, R., Quenby, S., 2013. A feasibility trial of screening women with idiopathic recurrent miscarriage for high uterine natural killer cell density and randomizing to prednisolone or placebo when pregnant. Human Reproduction 28, 1743–1752.